Using Eqs. (5) and (6), Eq. (4) reduces to

$$\phi_{c_3} = (\delta_{32} - 1)/[(2d_2/d_3)^{1/2} - 1] \quad (7)$$

From Eq. (7), $\phi_{c_3}$ can be estimated if $\delta_{32}$ is measured in a given experiment since $d_2$ and $d_3$ are known. However, for the particular value of $d_3/d_2 = 2$, $\phi_{c_3}$ cannot be found. Therefore, in Fig. 1 Eq. (7) is plotted over a wide range of the ratio $d_3/d_2$ to evaluate the best range of diameter ratios. Since $\delta_{32}$ is to be measured experimentally, it can be seen from Eq. (7) that it is better to have the value of $\delta_{32}$ as high as possible in order to obtain an accurate value of $\phi_{c_3}$. It can be seen from Fig. 1 that, for large values of $\delta_{32}$, diameter ratio $d_3/d_2$ should lie between 1.0 and 0.5. Ratios below 0.5 give rise to construction difficulties. The operating regime of the probe is shown by the hatched area in Fig. 1. Once $\phi_{c_3}$ is obtained in a given experiment, the velocity wall chemical reaction can also be estimated if the flow quantities $U$, $\rho$, $\mu$, etc. are known accurately. However, in the present method an accurate determination of $k_w$ is not necessary for measuring atom concentration.

### 2. Atom Concentration

A substitution of $\phi_{c_3}$ from Eq. (7) into Eq. (2) gives

$$(q_{c-nc})_3 = 0.763 S_c^{-0.63}(H_e - H_w) \times (\beta_3 \mu_e \rho_e)^{1/2}(h_R^\circ \alpha_\infty / H_e)\}(\delta_{32} - 1)/[(2d_2/d_3)^{1/2} - 1]\} \quad (8)$$

$\alpha_\infty$ can be found from Eq. (8) if $\mu$, $\rho$, and $U_\infty$ are known accurately, since $\delta_{32}$ and $(q_{c-nc})_3$ are measured in a given experiment. As noted previously, there are uncertainties in estimating these quantities. To avoid this, the following approach may be used.

Consider the heat-transfer equation to the noncatalytic gage in the three-dimensional model; since $\phi_{nc} \approx 0$,

$$(q_{nc})_3 = 0.763 P_r^{-0.63}(H_e - H_w)(\beta_3 \mu_e \rho_e)^{1/2}[1 - (h_R^\circ \alpha_\infty / H_e)] \quad (9)$$

Dividing Eq. (8) by Eq. (9) and rearranging

$$h_R^\circ \alpha_\infty / H_e = 1/[1 + \phi_{c_3} L_e^{0.63}(q_{nc}/q_{c-nc})_3] \quad (10)$$

where $\phi_{c_3}$ is estimated using Eq. (7).

To find $\alpha_\infty$ from Eq. (10), all of the quantities are measured except $Le$ and $He$. The Lewis number ($Le$) is usually taken as a constant for a given temperature,[6] and $He$ can be obtained fairly accurately from the reservoir conditions in a given hypersonic shock tunnel. Consequently, by using this approach, it is not essential to measure the flow quantities or the velocity of wall chemical reaction ($k_w$) of the gage in order to obtain the freestream atom concentration.

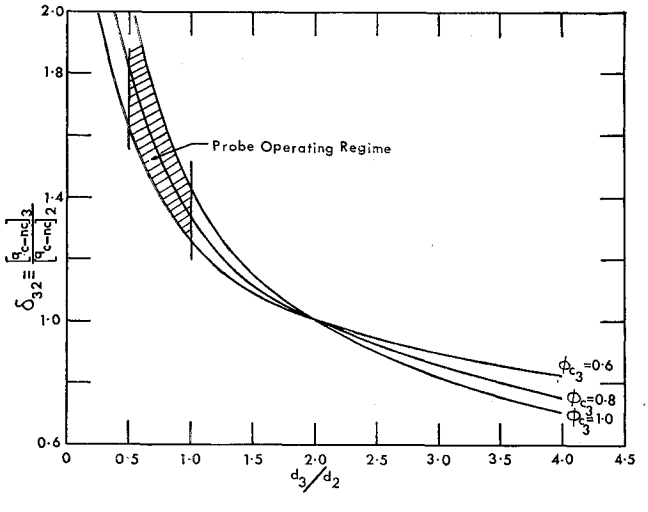


**Fig. 1 Variation of probe sensitivity with diameter ratios.**

Although the preceding analysis is valid strictly for blunt body flows with boundary layers that are separated from the shock wave by an inviscid shock layer, the analysis can also be extended to the cases when the flow Reynolds number is low enough to cause the now viscous shock layer and the boundary layer to merge. Using the Stanton number derived by Cheng,[7] a similar type of analysis has been done, and simple expressions for catalytic efficiency and freestream atom concentration have been derived. Thus this approach is applicable over a wide range of probe Reynolds number. This unique approach is being verified in the University of Toronto, Institute for Aerospace Studies 11- × 15-in. hypersonic shock tunnel.

### References

[1] Hartunian, R. A., "Local atom concentrations in hypersonic dissociated flows at low densities," Phys. Fluids **6**, 343–348 (1963).

[2] Goulard, R., "On catalytic recombination rates in hypersonic stagnation point heat-transfer," Jet Propulsion **28**, 737–745 (1958).

[3] Myerson, A. L., "Interim report on transient heat-transfer measurements of catalytic recombination in a step-function flow of atomic oxygen," Cornell Aeronautical Lab. Rept. AF-1412-A-2 (1962).

[4] Hartunian, R. A. and Liu, S. W., "Slow flow of a dissociated gas about a catalytic probe," Phys. Fluids **6**, 349–354 (1963).

[5] Hartunian, R. A. and Marrone, P. V., "Heat transfer from dissociated gases in a shock tube," Cornell Aeronautical Lab. Rept. AD-1118-A-7 (1959).

[6] Dorrance, W. H., *Viscous Hypersonic Flow* (McGraw-Hill Book Co., Inc., 1962), Chap. X, p. 308.

[7] Cheng, H. K., "Hypersonic shock-layer theory of the stagnation region at low Reynolds number," *Proceedings of the 1961 Heat Transfer and Fluid Mechanics Institute* (Stanford University Press, Stanford, Calif., 1961), p. 161.

# Nonzero Average Rate-Gyro Output from Sinusoidal Inputs

TAFT MURRAY*
*Avco Corporation, Wilmington, Mass.*

### Nomenclature

| | | |
|---|---|---|
| $B$ | = | rate-damping coefficient |
| $H_{IA}$, $H_{OA}$, $H_{SA}$ | = | angular momentum about the input, output, and spin axes |
| $H_W$ | = | angular momentum of gyro wheel |
| $I_{FIA}$, $I_{FOA}$, $I_{FSA}$ | = | moment of inertia of gyro float about input, output, and spin axes |
| $K$ | = | electrical or mechanical spring constant |
| $t_i$ | = | integration time |
| $\alpha_e$ | = | angular position error |
| $\Omega_{IA}$, $\Omega_{OA}$, $\Omega_{SA}$ | = | amplitude of sinusoidal angular rates about the input, output, and spin axes |
| $\theta$ | = | angular displacement between gyro float and case |
| $\omega_{EIR}$ | = | equivalent input angular rate |
| $\omega_{IA}$, $\omega_{OA}$, $\omega_{SA}$ | = | angular rates with respect to inertial space about the input, output, and spin axes |
| $\omega_n \equiv (K/I_{FOA})^{1/2}$ | = | gyro natural frequency |
| $\omega_V$ | = | frequency of sinusoidal angular rates |
| $\xi \equiv \frac{1}{2}B(I_{FOA}K)^{-1/2}$ | = | damping ratio |

Received October 21, 1964; revision received March 5, 1965.
* Senior Engineer, Guidance and Control Department, Research and Advanced Development Division.

SINUSOIDAL angular rates of identical frequencies about the input and spin axes of a rate-measuring gyro cause a nonzero average output. Although the angular rate error is negligible, the error in the integral of the rate signal may not be. For example, angular displacement information obtained by integrating rate-gyro signals during powered flight may be in error due to engine vibrations. An error expression and the magnitude of this error for a particular case will be derived.

Consider the structurally rigid model of a rate-measuring gyro shown in Fig. 1. From Newton's law $\mathbf{T} = d\mathbf{H}/dt$ about the mass center of the gyro float-wheel combination, the equation of motion about the output axis is

$$I_{FOA}\ddot{\theta} + B\dot{\theta} + K\theta = \omega_{IA}H_{SA} - \omega_{SA}H_{IA} - \dot{H}_{OA} \quad (1)$$

The angular momentum vectors as shown in Fig. 2 are

$$\left.\begin{aligned} H_{IA} &= (\omega_{IA}\cos\theta - \omega_{SA}\sin\theta)I_{FIA}\cos\theta + \\ &\quad H_W\sin\theta + (\omega_{SA}\cos\theta + \omega_{IA}\sin\theta)I_{FSA}\sin\theta \\ H_{SA} &= H_W\cos\theta + (\omega_{SA}\cos\theta + \omega_{IA}\sin\theta)I_{FSA}\times \\ &\quad \cos\theta - (\omega_{IA}\cos\theta - \omega_{SA}\sin\theta)I_{FIA}\sin\theta \\ \dot{H}_{OA} &= I_{FOA}\dot{\omega}_{OA} \end{aligned}\right\} \quad (2)$$

Substituting Eqs. (2) into Eq. (1) and making a small-angle $\theta$ approximation ($\sin\theta = \theta$, $\cos\theta = 1$, $\cos 2\theta = 1$), one obtains

$$I_{FOA}\ddot{\theta} + B\dot{\theta} + K'\theta = H_W\omega_{IA} - I_{FOA}\dot{\omega}_{OA} - (I_{FIA} - I_{FSA})\omega_{IA}\omega_{SA} \quad (3)$$

where

$$K' \equiv K + H_W\omega_{SA} + (I_{FIA} - I_{FSA})(\omega_{IA}^2 - \omega_{SA}^2)$$

Equation (3) is a linear equation with a time-varying spring term and three forcing functions. For a rate-measuring gyro with the following parameters:

$$I_{FOA} = 54 \text{ dyne-cm-sec}^2$$
$$H_W = 9 \times 10^4 \text{ dyne-cm-sec}$$
$$K = 57.3 \times 10^4 \text{ dyne-cm-rad}^{-1}$$
$$I_{FIA} - I_{FSA} < 50 \text{ dyne-cm-sec}^2$$

subjected to a rate vector with components

$$\omega_{SA} = \Omega_{SA}\sin\omega_V t$$
$$\omega_{IA} = \Omega_{IA}\sin\omega_V t$$
$$\omega_{OA} = \Omega_{OA}\sin\omega_V t$$

where, for example, $\Omega_{SA} \approx \Omega_{IA} \approx \Omega_{OA} \approx 1$ deg-sec$^{-1}$ and $\omega_V \approx 12$ rad-sec$^{-1}$, Eq. (3) is closely approximated by†

$$I_{FOA}\ddot{\theta} + B\dot{\theta} + [K + H_W\Omega_{SA}\sin\omega_V t]\theta = H_W\Omega_{IA}\sin\omega_V t \quad (4)$$

For a nonzero average output to exist, Eq. (4) shows that $\omega_{SA}$ and $\omega_{IA}$ must have identical frequencies over a period,

† The spring term $H_W\omega_{SA}$ is mentioned in Ref. 1.

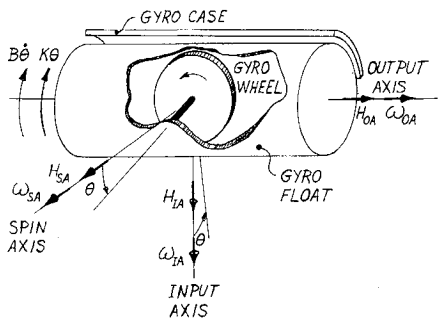


**Fig. 1 Structurally rigid gyro model.**

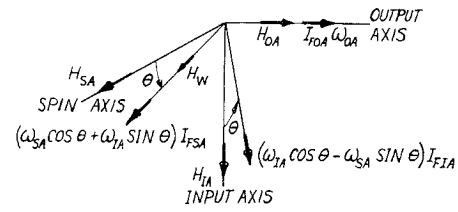


**Fig. 2 Angular momentum diagram.**

but the frequencies need not remain constant through time. The example of identical frequencies will now be continued.

It is convenient to define an equivalent input angular rate as

$$\omega_{EIR} = (K/H_W)\theta \quad (5)$$

Substituting Eq. (5) into Eq. (4), one obtains

$$\ddot{\omega}_{EIR} + 2\xi\omega_n\dot{\omega}_{EIR} + \left[\omega_n^2 + \frac{H_W}{I_{FOA}}\Omega_{SA}\sin\omega_V t\right]\omega_{EIR} = \omega_n^2\Omega_{IA}\sin\omega_V t \quad (6)$$

The perturbation method‡ will now be used to show that a nonzero average $\omega_{EIR}$ results from the sinusoidal inputs of $\omega_{SA}$ and $\omega_{IA}$. A series solution for $\omega_{EIR}$ is assumed in the form of

$$\left.\begin{aligned} \omega_{EIR} &= X_0 + (H_W\Omega_{SA}/I_{FOA})X_1 + (H_W\Omega_{SA}/I_{FOA})^2X_2 + \ldots \\ \omega_{EIR} &= \dot{X}_0 + (H_W\Omega_{SA}/I_{FOA})\dot{X}_1 + \ldots \\ \ddot{\omega}_{EIR} &= \ddot{X}_0 + (H_W\Omega_{SA}/I_{FOA})\ddot{X}_1 + \ldots \end{aligned}\right\} \quad (7)$$

Substituting Eqs. (7) into Eq. (6) and equating terms of equal powers of $H_W\Omega_{SA}/I_{FOA}$, one obtains for $(H_W\Omega_{SA}/I_{FOA})^0$

$$\ddot{X}_0 + 2\xi\omega_n\dot{X}_0 + \omega_n^2X_0 = \omega_n^2\Omega_{IA}\sin\omega_V t \quad (8)$$

and for $(H_W\Omega_{SA}/I_{FOA})^1$

$$\ddot{X}_1 + 2\xi\omega_n\dot{X}_1 + \omega_n^2X_1 = -X_0\sin\omega_V t \quad (9)$$

Solving for the particular solutions of Eqs. (8) and (9) and substituting these solutions into Eq. (7), one obtains

$$\omega_{EIR} = C\cos\omega_V t + D\sin\omega_V t + (H_W\Omega_{SA}/I_{FOA})[E\sin 2\omega_V t + F\cos 2\omega_V t - (D/2\omega_n^2)] \quad (10)$$

where

$$C = \frac{2\xi\omega_n^3\omega_V\Omega_{IA}}{(\omega_n^2 - \omega_V^2)^2 + (2\xi\omega_n\omega_V)^2}$$

$$D = \frac{\omega_n^2\Omega_{IA}(\omega_n^2 - \omega_V^2)}{(\omega_n^2 - \omega_V^2)^2 + (2\xi\omega_n\omega_V)^2}$$

$$E = \frac{2\xi\omega_n\omega_V D - \frac{1}{2}C(\omega_n^2 - 4\omega_V^2)}{(\omega_n^2 - 4\omega_V^2) + (4\xi\omega_n\omega_V)^2}$$

$$F = \frac{2\xi\omega_n\omega_V C + \frac{1}{2}D(\omega_n^2 - 4\omega_V^2)}{(\omega_n^2 - 4\omega_V^2) + (4\xi\omega_n\omega_V)^2}$$

If the rate-measuring gyro's electrical output representing $\omega_{EIR}$ is integrated for angular position information, then the average angular position error $\alpha_e$ will be

$$\alpha_e = -\frac{1}{2}\left(\frac{H_W\Omega_{SA}\Omega_{IA}}{I_{FOA}}\right)\left(\frac{\omega_n^2 - \omega_V^2}{(\omega_n^2 - \omega_V^2)^2 + (2\xi\omega_n\omega_V)^2}\right)t_i$$

The approximate $\alpha_e$ for the forementioned rate-measuring

‡ Also called method of Poincare.

gyro parameters and inputs for $t_i$ equal to 300 sec is

$$|\alpha_e| \approx \frac{1}{2}\frac{H_W\Omega_{SA}\Omega_{IA}}{K}t_i = \frac{1}{2}\frac{(9\times10^4)(1)(1)(300)}{(57.3)(57.3\times10^4)}$$

$$|\alpha_e| \approx 0.41°$$

The error will increase (or decrease) in proportion to the product of the amplitudes ($\Omega_{SA}\Omega_{IA}$) of the rates.

### Reference

[1] "A handbook on floated integrating gyros," Reeves Corp., p. 8 (1958).

# A Thermal Boundary-Layer Problem in Magnetohydrodynamics

JOHN FILLO*
*Syracuse University, Syracuse, N. Y.*

### Nomenclature

| | | |
|---|---|---|
| $C_p$ | = | coefficient of specific heat at constant pressure |
| $\mathbf{H}$ | = | magnetic-field vector, magnitude $H$ |
| $h_x$, $h_y$ | = | components of $H$ along $x$, $y$ |
| $Hx$, $Hy$ | = | dimensionless components, $Hx = h_x/H_\infty$, $Hy = h_y/H_\infty$ |
| $H_\infty$ | = | magnetic-field strength in undisturbed stream |
| $\mathbf{j}$ | = | electric-current-density vector, magnitude $j$ |
| $k$ | = | thermal conductivity |
| $L$ | = | reference length |
| $Pm$ | = | $H_\infty^2/4\pi\ C_p\ T_\infty$ |
| $Pr$ | = | Prandtl number, $uC_p/k$ |
| $Prm$ | = | magnetohydrodynamic Prandtl number, $4\pi\sigma\nu$ |
| $\mathbf{q}$ | = | velocity vector |
| $Re$ | = | Reynolds number, $UL/\nu$ |
| $Rm$ | = | magnetic Reynolds number, $4\pi\ U\sigma L$ |
| $T$ | = | temperature |
| $T_\infty$ | = | temperature in undisturbed stream |
| $U_\infty$ | = | undisturbed-stream speed |
| $u$, $v$ | = | components of $q$ in $x$, $y$ directions |
| $U$, $V$ | = | dimensionless components, $U = u/U_\infty$, $V = v/U_\infty$ |
| $x$, $y$ | = | boundary-layer coordinates |
| $X$, $Y$ | = | dimensionless coordinates, $X = x/L$, $Y = y/\delta_t L$ |
| $\delta_t$ | = | typical thermal boundary-layer thickness, dimensionless |
| $\nu$ | = | kinematic viscosity |
| $\rho$ | = | mass density |
| $\sigma$ | = | electrical conductivity |
| $\theta$ | = | dimensionless temperature, $\theta = T - T_\infty/T_\infty$ |

### Introduction

In Ref. 1, Sears studied a class of steady plane and axisymmetric magnetohydrodynamic flows known as the aligned-fields flow, i.e., flow in which the basic or undisturbed situation consists of a uniform parallel stream and a uniform magnetic field parallel to it.

The flow regime was split into three regions, namely, the potential flow, the inviscid layer where magnetohydrodynamics (MHD) effects are present, and a viscous sublayer. The boundary-layer equations pertinent to the inviscid magnetohydrodynamic boundary layer, as well as the viscous sublayer, were derived and discussed. Similar solutions were found for these equations. The object of this note is to derive and examine the thermal boundary-layer equations for steady plane aligned-fields flow.

Received February 8, 1965.

* Instructor, Department of Mechanical and Aerospace Engineering.

### Analysis

The thermal boundary-layer equations are derived for fluids subject to large magnetic Reynolds numbers, small magnetic Prandtl numbers, and Prandtl numbers of order one. In addition, we shall only consider constant-property fluids and incompressible flow.

The temperature distribution about a heated body may be found from the following equation:

$$\rho C_p(\mathbf{q}\cdot\nabla T) = k\nabla^2 T + \rho\nu\Phi + j^2/\sigma \tag{1}$$

where $T$ is the local temperature, $\mathbf{q}$ is the local velocity vector with components $u$, $v$ and is assumed to be known from Ref. 1, $\Phi$ is the viscous dissipation, and $j^2/\sigma$ is the Joule heating term.

In addition to the velocity vector $\mathbf{q}$, we need to know $\mathbf{j}$. The necessary equations are

$$\mathbf{j} = \sigma(\mathbf{q}\times\mathbf{H}) \tag{2}$$

$$4\pi\mathbf{j} = \text{curl}\ \mathbf{H} \tag{3}$$

Where electromagnetic units are employed, the electric field $E$ is taken to be zero, and the fluid is assumed to be nonmagnetic.

In order to talk about the thermal boundary layer, we must take into account the fact that the flow regime is split into three regions. In light of this, the following model for the study of the thermal effects about a solid body is proposed: 1) an undisturbed region where the temperature is $T_\infty$; 2) a magnetoinviscid-thermal layer where thermal conduction is negligible, and only convection and Joule heating contribute to the transport of thermal energy; and 3) a viscous-thermal layer where thermal conduction, convection, viscous, and Joule heating are important. This idea of splitting the thermal region was also considered in Ref. 2 but for an entirely different problem.

The justification for neglecting the heat transport by conduction in the magnetoinviscid-thermal layer rests on the fact that the fluids under consideration are those for which the heat conductivity is small. Thus, it is well known[3] that conduction becomes important only in the region where the convective heat transport is small because of small velocities, and this occurs in the region near the solid surface of the body, since the velocity goes to zero.

#### *Magneto-inviscid-thermal layer*

To derive the boundary-layer equations pertinent to this region, let us consider the following transformation to dimensionless variables:

$$X = x/L \qquad Y = y/L\delta_t$$

where $L\delta_t$ is a typical thickness of the boundary layer. In dimensionless form, Eq. (1) becomes

$$U\frac{\partial\theta}{\partial X} + \frac{V}{\delta_t}\frac{\partial\theta}{\partial Y} = \frac{Pm}{Rm}\left(\frac{\partial Hy}{\partial X} - \frac{1}{\delta_t}\frac{\partial Hx}{\partial Y}\right)^2 \tag{4}$$

As in Ref. 1 where all dependent variables are expressed in the form of a power series, we now assume that the nondimensional temperature $\theta$ may be expressed in the form of a power series in a small parameter that vanishes in the limit $Rm = \infty$, i.e.,

$$\theta = \sum_{n=0}^{\infty}\theta_n X^n \tag{5}$$

where

$$X^n = Rm^{-P} \qquad P > 0 \tag{6}$$

Absorbing the constant of proportionality in the definition of $\delta_t$, we assume that the dimensionless thermal boundary-